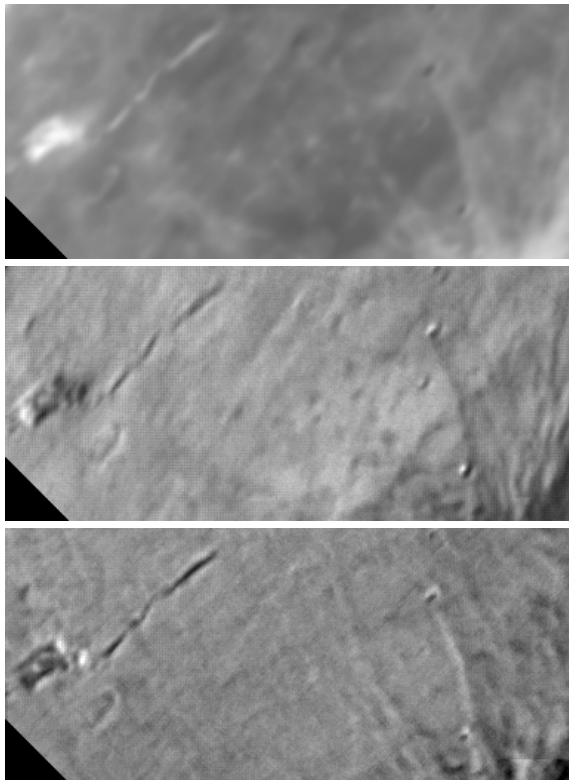


## POLARISATION ANGLE ANOMALIES OF LUNAR CRATER RAYS AND REINER GAMMA

C. Wöhler, Daimler Group Research, P. O. Box 2360, D-89013 Ulm, Germany; christian.woehler@daimler.com  
Geologic Lunar Research (GLR) Group

**Introduction:** Light reflected from the lunar surface is linearly polarised [1]. Measurements of the polarisation state yield information about the fine-structure of the lunar regolith. Relying on a calibration based on returned samples, the median grain size and the mean roughness slope angle can be determined from the surface albedo and the polarisation degree [2]. A soil maturity index can be inferred from the phase angle at which the light reflected from the lunar surface displays a maximum degree of linear polarisation [3]. Integrated over the lunar disk, the direction of polarisation is parallel to the Sun-Moon-Earth plane for phase angles below  $23.5^\circ$ , while for larger phase angles it is perpendicular to it [1]. In this contribution we describe small-scale deviations of the direction of polarisation from its average value. In the absence of topographic profile, such variations of the polarisation angle are observed for lunar crater rays. A similar distinct small-scale anomaly of the polarisation angle is displayed by the Reiner Gamma formation.



**Fig. 1:** Kepler rays (right) and Reiner Gamma (left). Top:  $I$ ; middle:  $D$  (grey value range 0.04–0.20); bottom:  $\Phi$  (grey value range  $\pm 15^\circ$ ). Decreasing grey value corresponds to positive angular variation w. r. t. the Sun-Moon-Earth plane.

**Measurement procedure:** The polarisation data were determined based on telescopic CCD images ac-

quired in the Johnson I (Figs. 1-5) and V (Fig. 6) bands through a linear polariser under relative orientation angles  $\omega$  of  $0^\circ$ ,  $45^\circ$ ,  $90^\circ$ ,  $135^\circ$ , and  $180^\circ$ . An image registration procedure [4] was applied to the images. The  $0^\circ$  and  $180^\circ$  images were utilised to determine the atmospheric absorption coefficient, which was then used to correct the average grey levels of the acquired images according to the corresponding differences in elevation above the horizon [5]. However, the influence of atmospheric absorption on the determined polarisation parameters was found to be minor. To each pixel, a sinusoidal function of the form  $I(\omega) = I_c + I_v \cos[2(\omega - \Phi)]$  was fitted using a linear least-mean-squares procedure. The value of  $I_c$  corresponds to the intensity, the polarisation degree is given by  $D = I_v/I_c$ , and the polarisation angle is defined as the polariser orientation angle  $\Phi$  under which the observed intensity is maximal [6]. This measurement technique allows to determine variations of the polarisation degree and angle on pixel scales. The zero level of  $\Phi$  is arbitrary. An error analysis reveals that under the (fairly pessimistic) assumption of a noise level of 1% for the pixel grey values, the standard error amounts to 0.007 for the polarisation degree  $D$ . The standard error of the polarisation angle depends on  $D$  and corresponds to  $2^\circ$  for a typical value of  $D = 0.1$ .

**Lunar crater rays:** Crater rays consist of material ejected during an impact event. They differ in maturity and/or composition from the surrounding soil [7]. We have examined the ray systems of Kepler (Fig. 1), Aristarchus (Fig. 2), and Proclus (Fig. 3) at phase angles of  $\alpha = 89.2^\circ$ ,  $113.6^\circ$ , and  $63.3^\circ$ , respectively; furthermore several rays at the western border of Oceanus Procellarum east of the craters Cardanus and Krafft (Fig. 4,  $\alpha = 89.2^\circ$ ) and the area immediately south of Seleucus in western Oceanus Procellarum (Fig. 5,  $\alpha = 147.2^\circ$ ). Bright crater rays display a lower polarisation degree than the surrounding surface [8]. In addition to that, we found that the polarisation angle differs by up to  $10^\circ$ – $20^\circ$  from the value measured for the surrounding surface. The behaviour of the polarisation angle is independent of whether the ray is situated on mare soil (Kepler, Aristarchus, rays near Cardanus and Krafft) or on highland soil (Proclus). The region south of Seleucus (Fig. 5), which presumably contains ejecta, displays an increased polarisation degree (indicating a large grain size [2]) and a faint pattern of linear polarisation angle anomalies. At bottom right, a ray unrelated to Seleucus is apparent.

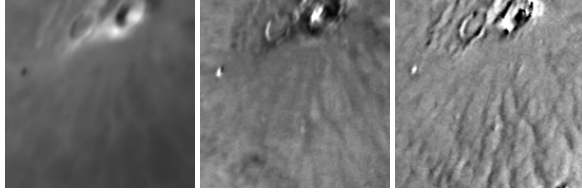


**Fig. 2:** Aristarchus ray system. Left:  $I_c$ ; middle:  $D$  (grey value range 0.00–0.20); right:  $\Phi$  (grey value range  $\pm 20^\circ$ ).

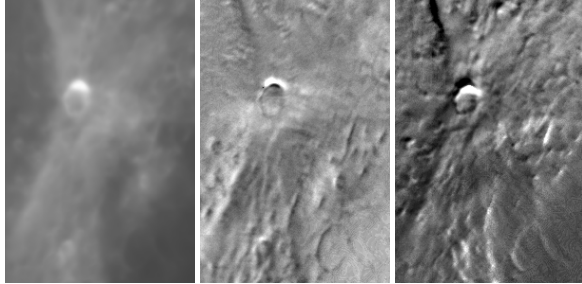


**Fig. 3:** Proclus ray system. Left:  $I_c$ ; middle:  $D$  (grey value range 0.00–0.10); right:  $\Phi$  (grey value range  $\pm 20^\circ$ ).

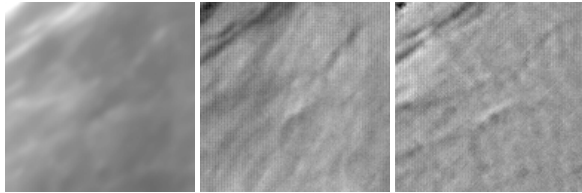


**Fig. 4:** Rays in western Oceanus Procellarum. Left:  $I_c$ ; middle:  $D$  (grey value range 0.04–0.20); right:  $\Phi$  (grey value range  $\pm 15^\circ$ ).

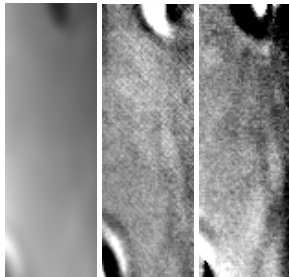


**Fig. 5:** Region south of Seleucus. Left:  $I_c$ ; middle:  $D$  (grey value range 0.04–0.09); right:  $\Phi$  (grey value range  $\pm 8^\circ$ ).

**Reiner Gamma:** Reiner Gamma is a swirl-like pattern of high albedo and without a topographic expression (cf. Fig. 1). It is located in western Oceanus Procellarum. Its main part consists of a bright ellipse, from which bright elongated patches extend into northeastern direction and small swirls to the southwest. All known lunar swirls are associated with magnetic anomalies ( $\sim 1000$  nT at the surface [9]), and some are antipodal to large impact structures. Their origin is still unknown. One explanation is that the swirls correspond to magnetised crustal or iron-rich ejecta material of basin impact origin, causing deflection of the solar wind and thus prevention of surface maturation [9].

Another possible origin is modification of the uppermost regolith layers by a cometary impact [10], where the magnetic field either formed during the impact or already existed and shielded the freshly exposed material from the solar wind [9]. It is shown in [11] that the high albedo of Reiner Gamma does not reflect a change in composition but is due to the immature soil. Our polarisation angle images of Reiner Gamma (cf. Figs. 1 and 6, acquired at phase angles of  $89.2^\circ$  and  $68.6^\circ$ , respectively), show strong correlations with albedo features and also with the photometric units established in [11], corresponding to surface regions with different physical properties. The polarisation angle patterns are similar to the phase ratio patterns reported in [12]. Specifically, the polarisation angle anomaly immediately south-east of the main ellipse, which appears bright in the right panel of Fig. 6, coincides with a backward-scattering patch interpreted in [12] as a region of anomalously high surface roughness.

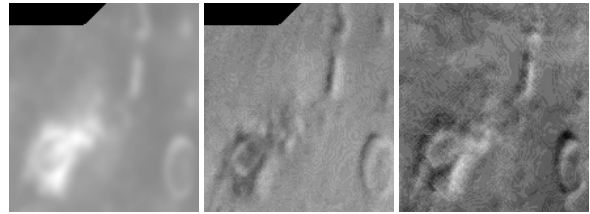


**Fig. 6:** Reiner Gamma. Left:  $I_c$  (V band); middle:  $\Phi$  (V band, grey value range  $\pm 12.5^\circ$ ); right:  $\Phi$  (I band, grey value range  $\pm 12.5^\circ$ ).

**Conclusion:** Lunar crater rays, the region south of Seleucus, and Reiner Gamma exhibit similar polarisation angle anomalies. The physical mechanism behind the observed polarisation angle anomalies remains unknown. For Reiner Gamma, the Faraday effect induced by the magnetic field is presumably too weak by several orders of magnitude to serve as an explanation. Possibly, the polarisation angle anomalies are induced by surface modifications due to the impact of small bodies (ejecta material for crater rays, micrometeoroids in the case of Reiner Gamma when assuming a cometary impact origin) – the occurrence of “herringbone” patterns in Reiner Gamma, characteristic for low-angle impacts, is mentioned in [9]. In this line of thought, the similarity between the polarisation angle anomalies of crater rays and Reiner Gamma strengthens the hypothesis that Reiner Gamma is an impact-related structure. Future work will address the relations between polarisation angle, wavelength, and illumination geometry.

**References:** [1] Lyot (1929) *Ann. Obs. Meudon VIII*; [2] Dollfus (1998) *Icarus 136*; [3] Shevchenko et al. (2004) *Solar System Research 37*; [4] Gottesfeld Brown (1992) *ACM Computing Surveys 24*; [5] Sterken and Manfroid (1992) *Kluwer Acad. Publ.*; [6] d’Angelo and Wöhler (2007) *ISPRS J. Photogrammetry and Remote Sensing*, in press; [7] Hawke et al. (2004) *Icarus 170*; [8] Dollfus (1999) *Icarus 140*; [9] Hood and Williams (1989) *LPSC XIX*; [10] Srnka and Schultz (1980) *LPSC XI*; [11] Chevrel et al. (2006) *LPSC XXXVII*; [12] Opananenko and Shkuratov (2004) *LPSC XXXV*.